Journal of Electronic Materials
https://doi.org/10.1007/s11664-024-10931-2

ORIGINAL RESEARCH ARTICLE

Highly Crystalline and Stoichiometric Growth of CdTe by Cost-Effective Hydrothermal Technique

Maruti V. Salve[1] · Aparna S. Ukarande[1] · O. I. Olusola[2] · T. M. W. J. Bandara[3] · M. Furlani[4] · B.-E. Mellander[4] · M. A. K. L. Dissanayake[5] · I. Albinsson[6] · Nandu B. Chaure[1]

Received: 7 August 2023 / Accepted: 11 January 2024

Abstract

CdTe powder samples have been synthesized using a hydrothermal approach, employing cadmium acetate and tellurium dioxides as sources of Cd and Te, respectively. $NaBH_4$ was utilized as the reducing agent, and double-distilled water was used as the solvent in the synthesis process. The effect of annealing on the synthesized samples was investigated. The samples have been characterized by x-ray powder diffraction, Raman spectroscopy, UV-Vis-NIR spectroscopy, scanning electron microscopy, energy dispersive spectroscopy, and x-ray photoelectron spectroscopy. The electrical properties (current–voltage and capacitance–voltage) of the as-prepared and annealed CdTe pellets were investigated. These findings indicate that annealing can lead to improvements in crystallinity, crystallite size, and electrical conductance. This paper presents a simple, cost-effective, and versatile method for producing significant amounts of CdTe nanostructure powders with properties suitable for use in the fabrication of CdS/CdTe solar cells.

Keywords Hydrothermal technique · CdTe · thin film · structural properties · stoichiometric growth

Introduction

Cadmium telluride (CdTe) is an emerging thin-film solar cell (TFSC) technology owing to its optimum optical energy band gap of 1.45 eV and high absorption coefficient ($> 10^5$ cm^{-1}) in the visible region.[1,2] The highest efficiency for CdS/CdTe thin film solar cells of ~ 22.1% has been reported by First Solar using the close space sublimation growth technique[3]. However, the reported efficiency is reasonably lower than the theoretical limit of 30% set by Schockley–Quiesser (S-Q) for single-heterojunction solar cells.[4] Several issues need to be resolved to achieve efficiency close to the S-Q limit, such as back low resistive contact to CdTe, highly crystalline less defective CdTe materials, the use of appropriate oxidation and reducing reagents to achieve Te-rich surfaces, etc. Surface defects, such as stacking faults, twins, and grain boundaries, can trap charge carriers, reduce carrier mobility, increase recombination, and limit the carrier lifetime.[5,6] These parameters can lead to a reduction in the performance of TFSC devices. Post-deposition annealing of CdTe surfaces with $CdCl_2$ treatment is widely used to reduce the defect density and TO improve cell performance.[7,8] Doping the CdTe with an appropriate dopant results in an improvement in its electrical properties, which reduces the recombination of charge carriers and improves its efficiency[9–12]. The performance of the devices is also strongly dependent on the surface morphology, chemical composition, and electrical properties of the CdTe materials.[13–15]

Several methods have been developed to synthesize high-quality CdTe samples, including thermal evaporation,[16,17] close space sublimation,[18] electron beam evaporation,[19] electrodeposition,[20] pulsed laser deposition,[21]

✉ Nandu B. Chaure
n.chaure@physics.unipune.ac.in

1 Department of Physics, Savitribai Phule Pune University, Pune 411007, India

2 Department of Physics, The Federal University of Technology Akure, Akure, Nigeria

3 Department of Physics and Postgraduate Institute of Science, University of Peradeniya, Peradeniya, Sri Lanka

4 Department of Physics, Chalmers University of Technology, Gothenburg, Sweden

5 National Institute of Fundamental Studies, Hantana Road, Kandy, Sri Lanka

6 Department of Physics, University of Gothenburg, Gothenburg, Sweden

Published online: 02 February 2024

spray pyrolysis[22], magnetron sputtering,[23] and colloidal techniques.[24,25] High-efficiency CdTe cells are generally prepared using vacuum-based techniques that produce highly compact, large-grain layers. However, the requirements for high-purity chemicals and sophisticated instrumentation increase capital investment. Moreover, these methods may not be easily transferable from laboratory to industrial-scale production. In addition, many of the aforementioned approaches may not always result in pure stoichiometric CdTe products containing excess Te as an impurity. These impurities can result in non-uniformity and defects in the CdTe structure, affecting its electronic and optical properties.[26,27] Among the various synthesis methods, the hydrothermal technique is commonly employed to prepare metal, semiconductor, and oxide samples owing to its simplicity, low cost, high reproducibility, relatively low temperature, and environmentally friendly process. The hydrothermal environment throws off impurities present in the reaction system.[28–30] Two approaches are commonly used to prepare colloidal CdTe nanostructures. One is the organometallic synthesis method,[31,32] which involves the high-temperature thermolysis of the precursors. However, a major limitation of this approach is the potential toxicity associated with the use of organometallic precursors in the synthesis process. The second approach is to grow CdTe colloidal nanostructures in an aqueous medium, which is simple, inexpensive, and less toxic.[33] Furthermore, this approach allows for precise control of the particle size and shape, morphology, stoichiometry, and crystallinity of the synthesized nanostructures by altering various reaction parameters, including temperature, reaction time, pH, pressure, reducing reagent, and precursor concentration.[34,35] Although sodium hydrogen tellurite (NaHTe) is a commonly used precursor in the aqueous synthesis of CdTe colloids, it is unstable and expensive.[25] An alternative, simpler approach involves the use of tellurium dioxide as a source of the Te precursor in the synthesis process. The synthesis of high-quality CdTe materials is essential to achieve high-performance CdTe TFSC devices.

We report a simple hydrothermal approach for the synthesis of CdTe nanostructures using cadmium acetate, tellurium dioxide, and $NaBH_4$ in an aqueous solution. We investigated the impact of post-deposition heat treatment on the physical and electrical properties of the CdTe samples. Approximately 250 mg of the CdTe powder sample was pressed into a round pellet at room temperature under a pressure of 5 tons, without an organic binder. Using the two-probe method, we performed current density–voltage and capacitance–voltage measurements for both as-prepared and annealed CdTe pellets (annealed at 400°C for 15 min). Our findings demonstrate that the annealing of CdTe samples results in an improvement in both the physical and electrical properties suitable for solar cell applications.

Experimental

The Te precursor solution, consisting of 0.04 mol TeO_2 , was prepared in 50 ml of double-distilled water (DDW) and was constantly stirred in a beaker. Then, 1 M NaOH solution was added dropwise to the milky-white TeO_2 suspension until it became a clear and transparent solution of sodium tellurite (solution A). A Cd precursor solution was prepared in another beaker using an aqueous solution of 0.04 mol cadmium acetate under constant stirring (solution B). Solutions A and B were heated to 60°C with continuous vigorous stirring. Subsequently, 80 mg $NaBH_4$ was added to the mixture. The obtained product was transferred to a sealed Teflon-lined stainless-steel autoclave and heated at 180°C in a muffle furnace for 24 h. After natural cooling, the precipitate was collected, and centrifuged, washed with DDW and ethanol at least five times, and the final suspension was dried in a hot-air oven. A dark gray powder was collected and thoroughly characterized.

Sample Characterization

The optical properties of the obtained products were studied using a JASCO V- 770 Uv-Vis-NIR spectrophotometer. The structural properties were studied using x-ray diffraction (XRD) with Cu $K\alpha$ radiation ($\lambda = 0.154$ nm). The microstructural properties were investigated using a micro-Raman spectrophotometer with an excitation wavelength of 785 nm (InViaRenishaw). The surface morphologies of the samples were investigated using scanning electron microscopy (SEM) with an operating voltage of 20 kV (JSM 6360-A; JEOL). The elemental compositions of the samples were determined using energy-dispersive spectroscopy (EDS) attached to the SEM unit. The chemical states and surface compositions of the samples were investigated using XPS (PHI 5000 Versaprobe-II; ULVAC-PHI). Current density–voltage and capacitance–voltage measurements were performed at room temperature using a two-probe method setup using a Biologic potentiostat with a booster facility to measure the current in a picoampere.

Reaction Mechanism

Solid cadmium acetate dissolved in DDW underwent dissociation into its constituent ions, Cd^{2+} and $(CH_3COO)^-$, which were uniformly distributed throughout the DDW. $(TeO_3)^{2-}$ was reduced to Te^{2-} ions from Na_2TeO_3 in the presence of $NaBH_4$, which reacted with Cd ions to form

CdTe. The following reactions occurred sequentially to form CdTe powder suspensions:

$$Cd(CH_3COO)_2.2H_2O + H_2O \rightarrow Cd^{2+} + 2(CH_3COO)^- + 3H_2O \quad (1)$$

$$TeO_2 + 2NaOH + 2H_2O \rightarrow Na_2TeO_3 + 3H_2O \quad (2)$$

$$(TeO_3)^{2-} + BH^{4-} \rightarrow Te^{2-} + H_2BO_3^{2-} + H_2 \uparrow \quad (3)$$

$$Cd^{2+} + Te^{2-} \rightarrow CdTe \quad (4)$$

Results and Discussion

X-ray Diffraction

The XRD patterns of the as-prepared and annealed CdTe powder samples are shown in Fig. 1. The reflection peaks observed at approximately 23.42°, 38.94°, 46.06°, and 56.49° were indexed to the Bragg diffraction planes (111), (220), (311), and (400), respectively, of the cubic crystal structure of CdTe.[20,36] It is noteworthy that impurity and metallic Te peaks were not observed in the XRD spectra of either the as-prepared or annealed samples, which indicates that the chemical reaction between the Cd and Te ions was completed within the optimized initial chemical contents, as well as the reaction time and temperature. The XRD pattern of the as-prepared powder samples exhibited broader peaks that could be associated with the growth of nano-sized particles, which was confirmed by the optical properties. Upon annealing, the crystallinity of the powder sample increased drastically, as confirmed by the values of the full width at half-maximum (FWHM). This improvement in crystallinity could be due to the increase in thermal energy during the annealing process, which assists in the movement of atoms to the proper lattice positions.[37,38] As a result, the defects are reduced and more orderly crystal structures are formed, which leads to recrystallization of the CdTe lattice.

The slight variation in the measured values of the interplanar distance, d, compared with its standard counterpart could be due to the strain present in the sample. The strain present on the sample and average crystallite size was calculated using the Williamson–Hall (W-H) equation[39]:

$$\beta \cos\theta = \frac{K\lambda}{D} + 4\varepsilon \sin\theta \quad (5)$$

where β is the FWHM, λ is the x-ray wavelength ($\lambda = 1.540$ Å), D is the average crystallite size, ε is the strain, and K is a shape-dependent constant.

The W-H plot of ($\beta\cos\theta$) versus ($4\sin\theta$) of the observed diffraction peaks is shown in Fig. 2. The y-intercept and slope of the fitted line give values of the average crystallite size and internal microstrain, respectively. The values of 'D' and 'ε' were calculated to be 18 nm and 51 nm and 0.0022 and 0.0015 for the as-prepared and annealed samples, respectively, and the positive values of strain obtained from the slope represent the presence of tensile strain in the crystal structure.[40] The average crystallite size was observed to be increased and the internal microstrain decreased for the annealed CdTe sample. An increase in crystallite size following the annealing process can be ascribed to enhanced surface mobility of small crystals coalescing to form large crystals.[41] The lattice strain arises due to the displacement of atoms from their reference lattice positions in a crystal lattice. The decrease in internal microstrain for the annealed sample revealed a reduction in the concentration of lattice imperfections.[42] These results are consistent with those reported by Khan et al. and Islam et al., where the authors reported that strains were released in annealed CdTe samples.[43,44] According to the literature, it has been documented

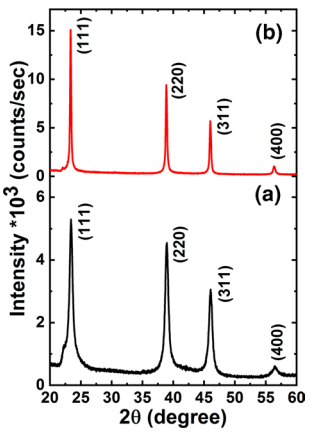

Fig. 1 XRD patterns of (a) as-prepared and (b) annealed CdTe nanostructure powder samples.

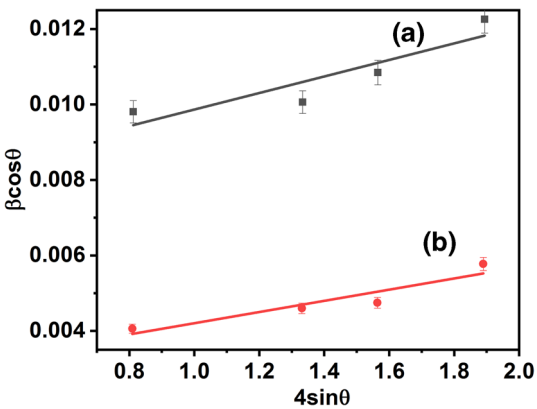

Fig. 2 W-H plot of (a) as-prepared and (b) annealed CdTe nanostructure samples.

Table I Structural parameters of CdTe nanostructure samples

Sample	2θ (degree)		Miller indices	FWHM (Rad.)	d (A°)		Phase assignment
	Standard	Observed			Standard	Observed	
As-prepared	23.75	23.42	(111)	0.0100	3.746	3.799	CdTe
	39.31	38.94	(220)	0.0106	2.290	2.313	CdTe
	46.43	46.06	(311)	0.0118	1.954	1.970	CdTe
	56.81	56.52	(400)	0.0139	1.621	1.628	CdTe
Annealed	23.75	23.35	(111)	0.0041	3.746	3.810	CdTe
	39.31	38.88	(220)	0.0049	2.290	2.317	CdTe
	46.43	46.02	(311)	0.0052	1.954	1.972	CdTe
	56.81	56.38	(400)	0.0066	1.621	1.632	CdTe

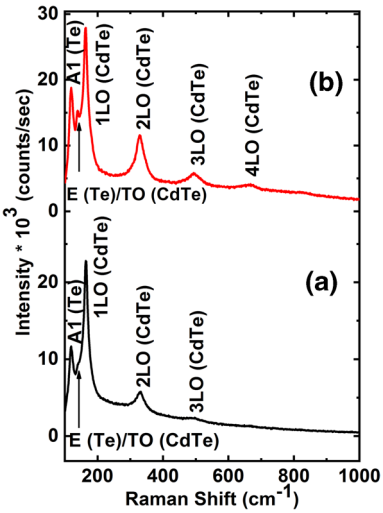

Fig. 3 Raman spectra of (a) as-prepared and (b) annealed CdTe nanostructure powder samples.

that the reductions in microstrain, dislocation density, and structural defects of annealed CdTe films result in an increase in crystallite size.[44–46] The values of the structural parameters are set out in Table I.

Raman Analysis

The microcrystalline behavior of the CdTe powder samples was investigated using Raman spectroscopy. The Raman spectra of the as-prepared and annealed samples at 785-nm excitation wavelength are depicted in Fig. 3. The peak observed at approximately 120 cm^{-1} was identified as the A1 phonon mode of Te. A small peak attributed to approximately 140 cm^{-1} was assigned to the transverse optical (TO) phonon mode of CdTe and the E phonon mode of Te. It has been reported that Te vibrational modes are typically seen in CdTe powder samples or films.[21,47] It has been observed that the TO phonon mode of CdTe becomes more distinguishable after annealing the sample, owing to enhancement in its crystallinity. The intense peak observed at about 164 cm^{-1} corresponds to the longitudinal optical (LO) phonon mode of CdTe and its multiple overtones 2LO, 3LO, and 4LO at about 328 cm^{-1}, 493 cm^{-1}, and 667 cm^{-1} , respectively. Researchers have reported that, when the energy of incoming or outgoing photons coincides with the band gap of the material, resonance Raman scattering occurs and, as a result, intense Raman spectra with several overtones arise.[48,49] The intensity ratio of 2-LO to 1-LO was calculated to determine the crystalline quality of the CdTe sample, and was found to be increased from 0.25 (as-prepared) to 0.41 (annealed), which revealed an improvement in the crystallinity of the CdTe samples. The Raman results were consistent with those of the XRD analysis.

Optical Properties

The optical properties of the CdTe samples were studied using UV-Vis-NIR diffuse reflectance spectroscopy. The Kubelka–Munk (K-M) Tauc relationship was used to estimate the optical energy band gap[50]:

$$\left[F\left(R_{\infty}\right).h\upsilon\right]^{2} = A\left(h\upsilon - E_{g}\right) \tag{6}$$

where h is Planck's constant, υ is the frequency, E_g is the energy band gap, A is the proportionality constant, and $F®_{\infty})$ is the K-M function, where R_{∞} is the absolute reflectance. The energy band gap of the CdTe sample was estimated from the plot of the K-M function $[F®).\ h\upsilon]^2$ versus $(h\upsilon)$ and extrapolating the linear portion of the graph to the energy axis, as shown in Fig. 4.

The estimated values of the optical energy band gap are 1.56 eV and 1.52 eV for the as-prepared and annealed samples, respectively. The sluggish behavior observed in both plots could be associated with the variation in particle size. Furthermore, the estimated value of E_g for the as-prepared sample was higher than that of the bulk counterpart because of the nanocrystalline particle size. The band gap decreased for the annealed CdTe sample, which could be due to the increase in the particle size and the improvement in the crystallinity of CdTe after annealing. According to previously

reported works, E_g decreases with annealing, which may be due to the increased grain size, grain realignment, and decreased internal microstrain.[51,52] In semiconductor materials, E_g can be influenced by several factors, such as carrier concentration, stoichiometric deviation, recrystallization, quantum confinement effects, dopants, and lattice strain.[53,54]

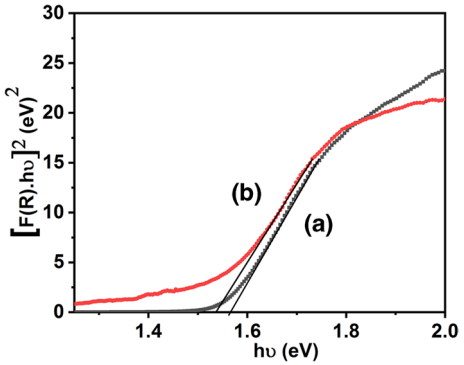

Fig. 4 K-M Tauc plots for (a) as-prepared (b) annealed CdTe nanostructure samples.

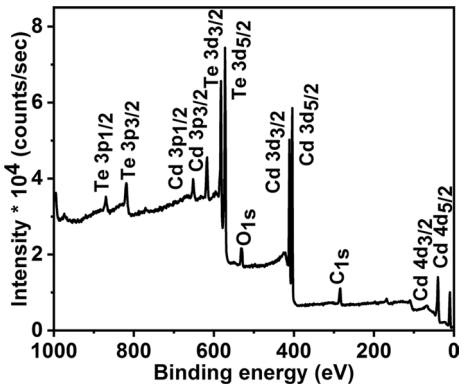

Fig. 5 XPS survey spectrum of annealed CdTe nanostructure samples.

The estimated values of the optical band gap are in close agreement with the standard value of the band gap of CdTe.

X-ray Photoelectron Spectroscopy

The chemical oxidation states were investigated using XPS analysis. The survey scan shown in Fig. 5 exhibits the presence of Cd, Te, O, and C in the CdTe. The carbon and oxygen peaks in the XPS spectrum may be due to surface contamination by the adsorbed gas molecules. The XPS data were standardized from the carbon peak observed at approximately 282 eV.[55] The core-level high-resolution XPS spectra of Cd and Te in the CdTe material are shown in Fig. 6a and b, respectively.

The Cd 3d peak observed at the binding energies of 404.06 and 410.76 correspond to Cd $3d_{5/2}$ and Cd $3d_{3/2}$, respectively, for Cd bonded to Te in CdTe. The Te $3d_{5/2}$and $Te3d_{3/2}$ peaks are divided into two peaks, one of which is connected to Cd-Te bonds and the other to Te-O bonds. The peaks Te $3d_{5/2}$ and Te $3d_{3/2}$ at binding energies of 571.50 eV and 581.96 eV, respectively, represent Te^{-2} states in CdTe. Additional peaks observed at 574.86 eV and 585.28 eV corresponding to Te^{4+} states within Te-O bonds in TeO_2 can be attributed to oxidation of the CdTe surface. These findings are in good agreement with those of previous studies.[55,56]

Scanning Electron Microscopy

The SEM images of the as-prepared and annealed CdTe nanostructure samples in Fig. 7 show globular grain morphology. The particles were more regular in the as-prepared CdTe sample and slightly irregular in the annealed CdTe sample. As shown in Fig. 7b and d, ImageJ software was used to calculate the particle size and distribution. Fifty particles were analyzed to determine the length of the individual particles. The average particle sizes of the as-prepared and annealed CdTe samples were 111 nm and

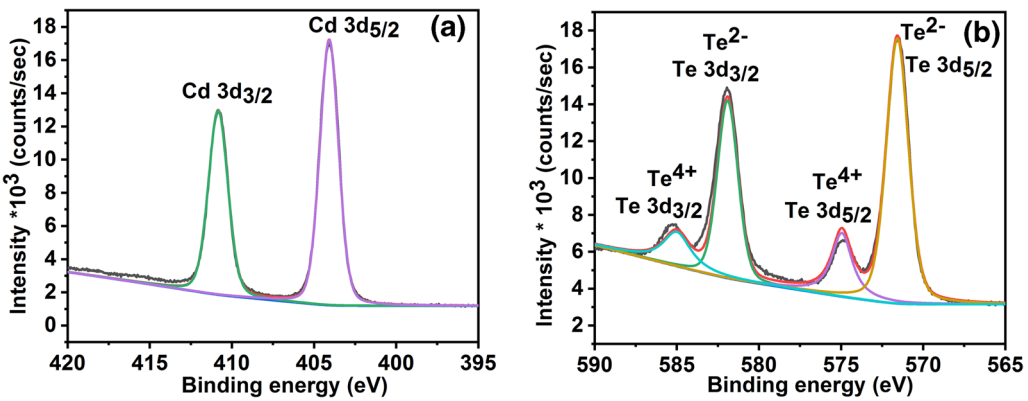

Fig. 6 XPS core level spectra of annealed CdTe nanostructure samples: (a) Cd 3d, (b) Te 3d.

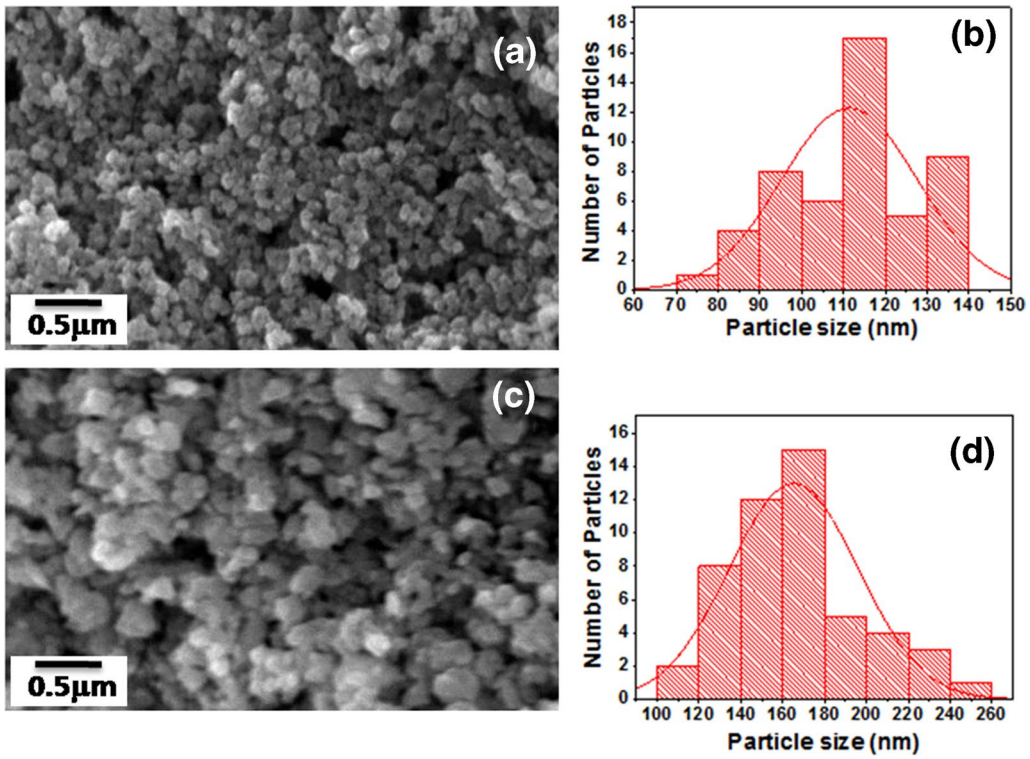

Fig. 7 (a) SEM image and (b) histogram depicting the distribution of particle sizes for the as-prepared CdTe powder samples. (c) SEM image and (d) histogram depicting the distribution of particle sizes for the annealed CdTe powder samples.

Table II Compositional analysis of as-prepared and annealed CdTe powder samples

Sample	Elemental atomic percentage (%) composition	
	Cd	Te
As prepared	48	52
Annealed	51	49

165 nm, respectively, showing that the average particle size increased for the annealed CdTe samples. Previous studies have reported that increasing the temperature promotes grain growth, resulting in larger grain sizes,[7,14] which is primarily attributed to the higher atomic mobility, which enables more atoms to coalesce to form larger grains.[38] In addition, an increased particle size distribution was observed for the annealed CdTe sample. This can be attributed to coalescence and/or recrystallization during the annealing process. The observed morphology demonstrates the potential applications of CdTe thin-film solar cells.

The elemental chemical composition was determined using EDS analysis, and the results are presented in Table II. EDS was performed at three different locations, and the average elemental atomic percentage compositions of Cd and Te were determined for the as-prepared and annealed CdTe powder samples. The EDS analysis showed that the as-prepared CdTe samples exhibited a slight excess of Te composition. However, during annealing, structural changes occurred in the CdTe sample, leading to a nearly stoichiometric composition. According to the analysis, it can be inferred that annealing significantly affects both the morphology and composition of the CdTe sample.

Current Density–Voltage Characteristics

The current density–voltage measurements of the as-prepared and annealed CdTe nanostructure samples are shown in Fig. 8. The measurements were performed on circular pellets with a diameter of 5 mm, which were obtained using a hydraulic press under a pressure of 5 t for 10 min at room temperature with no organic binder.

To make metal contact, graphite paste was applied to the pellets. It was observed that the current increases in the annealed CdTe sample, while the as-prepared CdTe sample contained lattice defects. This lattice defects along with the grain boundary area form carrier trap states which confine the free charge carriers by trapping them.[57] After thermal heat treatment, lattice defects and grain boundaries could be reduced due to the increase of crystallinity and crystallite size. As result, there were more available free charge carriers for electrical conduction.[58,59] In addition, charged traps

at grain boundaries create a potential energy barriers. The potential energy barrier hinders movement of free charge carriers across the grain boundaries, while the reduction of grain boundaries decreases the impact of charged traps at the boundaries, improving the current by enhancing mobility.[57] The current density–voltage measurements were used to determine the potential barrier height and ideality factor using[55]:

$$\Phi_{b0} = \frac{kT}{q}\ln\left(\frac{AA^*T^2}{I_0}\right) \tag{7}$$

$$\eta = \left(\frac{q}{kT}\right)\left(\frac{dV}{d(\ln I)}\right) \tag{8}$$

where A is the contact area, η is the ideality factor, Φ_{b0} is the potential barrier height, and V is the applied voltage. The values of η and Φ_{b0} were determined from the slope and intercept of the linear region of the ln(I) versus voltage (V) plot shown in Fig. 9. The calculated values of Φ_{b0}, η for the as-prepared and annealed CdTe samples are 0.59 eV, 3.22 eV, and 0.56 eV, 4.31, respectively.

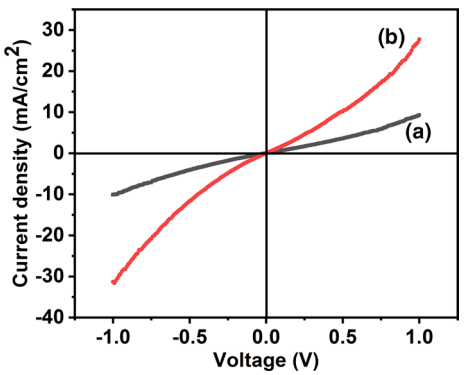

Fig. 8 Current–density versus voltage measurements of the (a) as-prepared and (b) annealed CdTe samples.

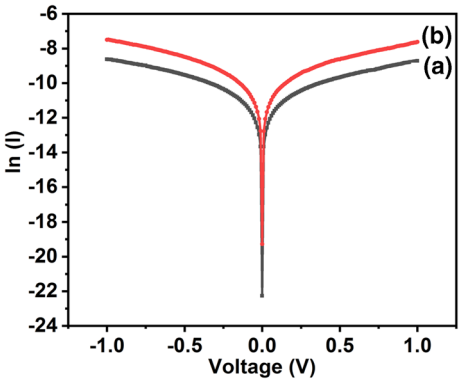

Fig. 9 ln(I) versus voltage plot of (a) as-prepared and (b) annealed CdTe samples.

An ideality factor $\eta > 1$ represents a departure from the ideal diode. Conduction mechanisms, generation–recombination currents, tunneling, and electrostatic image forces can cause ideality factors greater than one.[60,61] A decrease in the grain boundaries and the defects at the grain boundaries were observed in the annealed CdTe sample, which leads to an affect on the concentration of free charge carriers at the interface, lowering Φ_{b0} and correspondingly increasing the ideality factor (η).[58,62,63] According to some researchers, the number of charge carriers increases with the annealing temperature. The immobile charge on the semiconductor portion near the interface was neutralized by the free-charge carriers, which is the reason for the reduction in Φ_{b0}, and, consequently, the increase in η.[61,64] A decrease in the barrier height may be supported by the corresponding increase in the current.

Capacitance–Voltage Measurements

The capacitance–voltage was measured at a frequency of 100 KHz and the corresponding Mott–Schottky (M-S) ($1/C^2$ vs. V) plots of the as-prepared and annealed CdTe pellets are shown in Fig. 10.

The M-S plot shows three distinct regions: accumulation, depletion, and inversion. The capacitance of a graphite/CdTe pellet/graphite device can be expressed as[65]:

$$\frac{1}{C^2} = \frac{2(V_b + V - kT/q)}{q\varepsilon_0\varepsilon_S A^2 N_A} \tag{9}$$

where V_b is the flat-band potential, which can be determined from the extrapolation of the M-S (C^{-2} vs. V) plot to the x-axis, V is the applied voltage, A is the contact area, ε_s is the static dielectric constant of CdTe (~10.2), and ε_0 is the permittivity of free space. The net carrier concentration, N_A, was determined from the slope of the C^{-2} versus V plot and can be obtained from[39]:

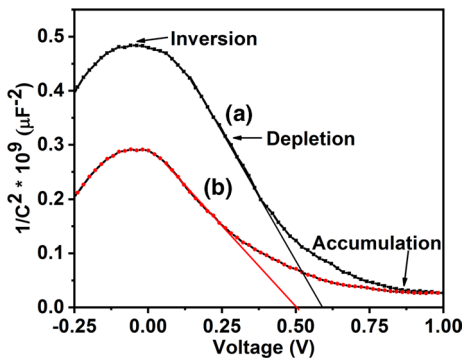

Fig. 10 Capacitance versus voltage measurements of (a) as-prepared and (b) annealed CdTe samples.

Table III Electrical parameters of a graphite/CdTe/graphite device calculated from capacitance–voltage and current density–voltage measurements

Sample	Ideality factor	Barrier height (eV)	Carrier concentration × 10^{13}/cm^3	Flat-band potential (V)
As-prepared	3.22	0.59	4.78	0.58
Annealed	4.31	0.56	7.42	0.50

$$N_A = \frac{2}{q\varepsilon_s\varepsilon_0 A^2}\left[\frac{1}{d(C^{-2})/dV}\right] \quad (10)$$

An increase in N_A and a decrease in V_b were observed for the annealed CdTe sample. The flat-band potential and carrier concentration values are listed in Table III. As shown in Fig. 10, the junction capacitance of the annealed CdTe sample increased, which could be due to an increase in carrier concentration that results in a reduction in the depletion region and, consequently, an increase in capacitance value.[63,66] The capacitance–voltage results agree with the current density–voltage measurements.

Conclusions

A simple hydrothermal method was used to produce CdTe nanostructure powder samples. The synthesis process involves the use of cadmium acetate, tellurium dioxide, and $NaBH_4$ as reducing agents in double-distilled water as the solvent. The results showed nearly stoichiometric growth of the CdTe nanostructure samples. Annealing the CdTe sample can substantially improve the crystallinity, crystallite size, carrier concentration, and electrical conductance. The physical properties of the CdTe nanostructure samples exhibited a significant dependence on annealing. The results of this study suggest that the obtained CdTe nanostructure samples exhibit favorable physical properties that make them suitable for cost-effective application in CdS/CdTe solar cells.

Acknowledgment The authors acknowledge the financial support received from the SERB, Ref. No.CRG/2018/000599. The authors are grateful to the Swedish Research Council (Grant Ref. Dnr. 2021-04889) for financial assistance under the Swedish Research Links Network between Sweden, India, Sri Lanka, and Nigeria. M.V.S. is grateful to the BANRF, 2020 for financial support.

Data Availability All data generated or analyzed during this study are included in this manuscript.

Conflict of interest The authors declare that they have no conflict of interest.

References

1. T.D. Lee and A.U. Ebong, A review of thin film solar cell technologies and challenges. *Renew. Sust. Energ. Rev.* 70, 1286 (2017). https://doi.org/10.1016/j.rser.2016.12.028.
2. B.M. Başol and B. McCandless, Brief review of cadmium telluride-based photovoltaic technologies. *J. Photonics Energy* 4(1), 040996 (2014). https://doi.org/10.1117/1.JPE.4.040996.
3. First Solar achieves an efficiency of 22.1% with their CdTe solar cell accessible online https://optics.org/news/7/2/29 (available online on 16/06/2023)
4. W. Shockley and H.J. Queisser, The Shockley-Queisser limit. *J. Appl. Phys.* 32(3), 510 (1961).
5. A. Kanevce, M.O. Reese, T.M. Barnes, S.A. Jensen, and W.K. Metzger, The roles of carrier concentration and interface, bulk, and grain-boundary recombination for 25% efficient CdTe solar cells. *J. Appl. Phys.* (2017). https://doi.org/10.1063/14984320.
6. S.H. Yoo, K.T. Butler, A. Soon, A. Abbas, and J.M.A. Walls, Walsh, identification of critical stacking faults in thin-film CdTe solar cells. *Appl. Phys. Lett.* (2014). https://doi.org/10.1063/14892844.
7. M.A. Islam, M.S. Hossain, M.M. Aliyu, M.R. Karim, T. Razykov, K. Sopian, and N. Amin, Effect of CdCl2 treatment on structural and electronic property of CdTe thin films deposited by magnetron sputtering. *Thin Solid Films* 546, 367 (2013). https://doi.org/10.1016/j.tsf.2013.04.067.
8. N. Spalatu, J. Hiie, V. Valdna, M. Caraman, N. Maticiuc, V. Mikli, T. Potlog, M. Krunks, and V. Lughi, Properties of the $CdCl_2$ air-annealed CSS CdTe thin films. *Energy Proc.* 44, 85 (2014). https://doi.org/10.1016/j.egypro.2013.12.013.
9. S.L. Patel, A. Thakur, M.D. Kannan, and M.S. Dhaka, Analysis of different annealing conditions on physical properties of Bi doped CdTe thin films for potential absorber layer in solar cells. *Sol. Energy* 199, 772 (2020). https://doi.org/10.1016/j.solener.2020.02.066.
10. W.K. Metzger, S. Grover, D. Lu, E. Colegrove, J. Moseley, C.L. Perkins, X. Li, R. Mallick, W. Zhang, R. Malik, J. Kephart, C.-S. Jiang, D. Kuciauskas, D.S. Albin, M.M. Al-Jassim, G. Xiong, and M. Gloeckler, Exceeding 20% efficiency with in situ group V doping in polycrystalline CdTe solar cells. *Nat. Energy* 4(10), 837 (2019). https://doi.org/10.1038/s41560-019-0446-7.
11. L. Kranz, C. Gretener, J. Perrenoud, R. Schmitt, F. Pianezzi, F. La Mattina, P. Blösch, E. Cheah, A. Chirilă, C.M. Fella, H. Hagendorfer, T. Jäger, S. Nishiwaki, A.R. Uhl, S. Buecheler, and A.N. Tiwari, Doping of polycrystalline CdTe for high-efficiency solar cells on flexible metal foil. *Nat. Commun.* 4(1), 2306 (2013). https://doi.org/10.1038/ncomms3306.
12. T.A. Fiducia, B.G. Mendis, K. Li, C.R. Grovenor, A.H. Munshi, K. Barth, W.S. Sampath, L.D. Wright, A. Abbas, J.W. Bowers, and J.M. Walls, Understanding the role of selenium in defect passivation for highly efficient selenium-alloyed cadmium telluride solar cells. *Nat. Energy* 4(6), 504 (2019). https://doi.org/10.1038/s41560-019-0389-z.
13. T.M. Razykov, G. Contreras-Puente, G.C. Chornokur, M. Dybjec, Y. Emirov, B. Ergashev, C.S. Ferekides, A. Hubbimov, B. Ikramov, K.M. Kouchkarov, X. Mathew, D. Morel, S. Ostapenko, E. Sanchez-Meza, E. Stefanakos, H.M. Upadhyaya, O. Vigil-Galan, and Y.V. Vorobiev, Structural, photoluminescent and electrical properties of CdTe films with different compositions fabricated by CMBD. *Sol. Energy* 83(1), 90 (2009). https://doi.org/10.1016/j.solener.2008.07.003.
14. N. Spalatu, J. Hiie, V. Mikli, M. Krunks, V. Valdna, N. Maticiuc, T. Raadik, and M. Caraman, Effect of CdCl2 annealing treatment on structural and optoelectronic properties of close spaced sublimation CdTe/CdS thin film solar cells versus deposition

conditions. *Thin Solid Films* 582, 128 (2015). https://doi.org/10.1016/j.tsf.2014.11.066.
15. D. Krasikov and I. Sankin, Defect interactions and the role of complexes in the CdTe solar cell absorber. *J. of Mater. Chem. A.* 5(7), 3503 (2017). https://doi.org/10.1039/C6TA09155E.
16. S. Singh, R. Kumar, and K.N. Sood, Structural and electrical studies of thermally evaporated nanostructured CdTe thin films. *Thin Solid Films* 519(3), 1078 (2010). https://doi.org/10.1016/j.tsf.2010.08.047.
17. V.V. Brus, M.N. Solovan, E.V. Maistruk, I.P. Kozyarskii, P.D. Maryanchuk, K.S. Ulyanytsky, and J. Rappich, Specific features of the optical and electrical properties of polycrystalline CdTe films grown by the thermal evaporation method. *Phys. Solid State* 56, 1947 (2014). https://doi.org/10.1134/S1063783414100072.
18. J. Schaffner, M. Motzko, A. Tueschen, A. Swirschuk, H.J. Schimper, A. Klein, T. Modes, O. Zywitzki, and W. Jaegermann, 12% efficient CdTe/CdS thin film solar cells deposited by low-temperature close space sublimation. *J. Appl. Phys.* (2011). https://doi.org/10.1063/13639291.
19. K. Punitha, R. Sivakumar, C. Sanjeeviraja, V. Sathe, and V. Ganesan, Physical properties of electron beam evaporated CdTe and CdTe: Cu thin films. *J. of Appl. Phys.* (2014). https://doi.org/10.1063/14903320.
20. H.I. Salim, V. Patel, A. Abbas, J.M. Walls, and I.M. Dharmadasa, Electrodeposition of CdTe thin films using nitrate precursor for applications in solar cells. *J. Mater. Sci.: Mater. Electr.* 26, 3119 (2015). https://doi.org/10.1007/s10854-015-2805-x.
21. F. de Moure-Flores, J.G. Quiñones-Galván, A. Guillén-Cervantes, J.S. Arias-Cerón, A. Hernández-Hernández, J. Santoyo-Salazar, J. Santos-Cruz, S.A. Mayén-Hernández, M.D. Olvera, J.G. Mendoza-Álvarez, and M. Meléndez-Lira, CdTe thin films grown by pulsed laser deposition using powder as target: effect of substrate temperature. *J. Cryst. Growth* 386, 27 (2014). https://doi.org/10.1016/j.jcrysgro.2013.09.036.
22. S.D. Gunjal, Y.B. Khollam, S.R. Jadkar, T. Shripathi, V.G. Sathe, P.N. Shelke, M.G. Takwale, and K.C. Mohite, Spray pyrolysis deposition of p-CdTe films: Structural, optical and electrical properties. *Sol. Energy* 106, 56 (2014). https://doi.org/10.1016/j.solener.2013.11.029.
23. F. Hosseinpanahi, D. Raoufi, K. Ranjbarghanei, B. Karimi, R. Babaei, and E. Hasani, Fractal features of CdTe thin films grown by RF magnetron sputtering. *Appl. Surf. Sci.* 357, 1843 (2015). https://doi.org/10.1016/j.apsusc.2015.09.048.
24. S. Wageh, A.M. Al-Amri, and A. Al-Ghamdi, Effect of adding reducing agent on the structure and optical properties of one-pot preparation method of CdTe quantum dots. *J. Mater. Sci.: Mater. Electr.* 27, 8384 (2016). https://doi.org/10.1007/s10854-016-4850-5.
25. F. Liu, S. Laurent, L. Vander Elst, and R.N. Muller, Synthesis of CdTe QDs by hydrothermal method, with tunable emission fluorescence. *Mater. Res. Exp.* 2(9), 095901 (2015). https://doi.org/10.1088/2053-1591/2/9/095901.
26. I.M. Dharmadasa, O.K. Echendu, F. Fauzi, N.A. Abdul-Manaf, O.I. Olusola, H.I. Salim, M.L. Madugu, and A.A. Ojo, Improvement of composition of CdTe thin films during heat treatment in the presence of $CdCl_2$. *J. Mater. Sci. Mater. Electron.* 28, 2343–2352 (2017). https://doi.org/10.1007/s10854-016-5802-9.
27. J.J. McCoy, S. Kakkireni, G. Gélinas, J.F. Garaffa, S.K. Swain, and K.G. Lynn, Effects of excess Te on flux inclusion formation in the growth of cadmium zinc telluride when forced melt convection is applied. *J. Cryst. Growth* 535, 125542 (2020). https://doi.org/10.1016/j.jcrysgro.2020.125542.
28. M. Sinha, R. Mahapatra, B. Mondal, T. Maruyama, and R. Ghosh, Ultrafast and reversible gas-sensing properties of ZnO nanowire arrays grown by hydrothermal technique. *J. Phys. Chem. C* 120(5), 3019 (2016). https://doi.org/10.1021/acs.jpcc.5b11012.
29. U. Pal and P. Santiago, Controlling the morphology of ZnO nanostructures in a low-temperature hydrothermal process. *J. of Phys. Chem. B.* 109(32), 15317 (2005). https://doi.org/10.1021/jp052496i.
30. C. Li, Z. Zang, C. Han, Z. Hu, X. Tang, J. Du, Y. Leng, and K. Sun, Highly compact $CsPbBr_3$ perovskite thin films decorated by ZnO nanoparticles for enhanced random lasing. *Nano Energy* 40, 195 (2017). https://doi.org/10.1016/j.nanoen.2017.08.013.
31. L. Algieri, R. Rosato, M.E. Mosca, M.L. Protopapa, A.G. Scalone, F. Di Benedetto, L. Bucci, and L. Tapfer, Green light-emitting CdTe nanocrystals: synthesis and optical characterizations. *Phys. Status Solidi C C* 12(1–2), 147 (2015). https://doi.org/10.1002/pssc.201400203.
32. P.V. Nair and K.G. Thomas, Hydrazine-induced room-temperature transformation of CdTe nanoparticles to nanowires. *J. Phys. Chem. Lett.* 1(14), 2094 (2010). https://doi.org/10.1021/jz100568p.
33. C. Wang, H. Zhang, S. Xu, N. Lv, Y. Liu, M. Li, H. Sun, J. Zhang, and B. Yang, Sodium-citrate-assisted synthesis of aqueous CdTe nanocrystals: giving new insight into the effect of ligand shell. *J. Phys. Chem. C* 113(3), 827 (2009). https://doi.org/10.1021/jp8088897.
34. G. Amin, M.H. Asif, A. Zainelabdin, S. Zaman, O. Nur, and M. Willander, Influence of pH, precursor concentration, growth time, and temperature on the morphology of ZnO nanostructures grown by the hydrothermal method. *J. Nanomater.* 2011, 5 (2011). https://doi.org/10.1155/2011/269692.
35. H. Wang, S. Cao, B. Yang, H. Li, M. Wang, X. Hu, K. Sun, and Z. Zang, NH_4Cl-modified ZnO for high-performance $CsPbIBr_2$ perovskite solar cells via low-temperature process. *Sol. Rrl.* 4(1), 1900363 (2020). https://doi.org/10.1002/solr.201900363.
36. G.R. Bhand and N.B. Chaure, Synthesis of CdTe, CdSe and CdTe/CdSe core/shell QDs from wet chemical colloidal method. *Mater. Sci. Semicond. Process.* 68, 279 (2017). https://doi.org/10.1016/j.mssp.2017.06.033.
37. R.A. Ismail, Effect of rapid thermal annealing on properties of thermally evaporated nanostructured CdTe thin film treated with $CdCl_2$. *Mater. Sci. Semicond. Process.* 15(2), 159 (2012). https://doi.org/10.1016/j.mssp.2011.10.005.
38. K. Punitha, R. Sivakumar, C. Sanjeeviraja, and V. Ganesan, Influence of post-deposition heat treatment on optical properties derived from UV–vis of cadmium telluride (CdTe) thin films deposited on amorphous substrate. *Appl. Surf. Sci.* 344, 89 (2015). https://doi.org/10.1016/j.apsusc.2015.03.095.
39. S.M. Sonawane, S. Chaure, and N.B. Chaure, Characterization of Sb_2Te_3 thin films prepared by electrochemical technique. *J. Phys. Chem. Solids* 172, 111095 (2023). https://doi.org/10.1016/j.jpcs.2022.111095.
40. P.U. Londhe and N.B. Chaure, Effect of pH on the properties of electrochemically prepared ZnO thin films. *Mater. Sci. Semicond. Proc.* 60, 5 (2017). https://doi.org/10.1016/j.mssp.2016.12.005.
41. M. Caglar and S. Ruzgar, Influence of the deposition temperature on the physical properties of high electron mobility ZnO films by sol–gel process. *J. Alloys Compd.* 644, 101 (2015). https://doi.org/10.1016/j.jallcom.2015.04.167.
42. M. Dongol, A. El-Denglawey, M.S. Abd El Sadek, and I.S. Yahia, Thermal annealing effect on the structural and the optical properties of Nano CdTe films. *Optik* 126(14), 1352 (2015). https://doi.org/10.1016/j.ijleo.2015.04.048.
43. N.A. Khan, K.S. Rahman, K.A. Aris, A.M. Ali, H. Misran, M. Akhtaruzzaman, S.K. Tiong, and N. Amin, Effect of laser annealing on thermally evaporated CdTe thin films for photovoltaic absorber application. *Sol. Energy* 173, 1051 (2018). https://doi.org/10.1016/j.solener.2018.08.023.
44. M.A. Islam, Q. Huda, M.S. Hossain, M.M. Aliyu, M.R. Karim, K. Sopian, and N. Amin, High quality 1 μm thick CdTe absorber

layers grown by magnetron sputtering for solar cell application. *Curr. Appl. Phys.* 13, S115 (2013). https://doi.org/10.1016/j.cap.2013.02.015.
45. P.K. Kumarasinghe, A. Dissanayake, B.M. Pemasiri, and B.S. Dassanayake, Effect of post deposition heat treatment on microstructure parameters, optical constants and composition of thermally evaporated CdTe thin films. *Mater. Sci. Semicond. Process.* 58, 51 (2017). https://doi.org/10.1016/j.mssp.2016.11.028.
46. S.N. Vidhya, O.N. Balasundaram, and M. Chandramohan, The effect of annealing temperature on structural, morphological and optical properties of CdZnTe thin films. *Optik* 126(24), 5460 (2015). https://doi.org/10.1016/j.ijleo.2015.09.032.
47. D. Wang, Y. Yang, T. Guo, X. Xiong, Y. Xie, K. Li, B. Li, and M. Ghali, Effect of pulse bias voltages on performance of CdTe thin film solar cells prepared by pulsed laser deposition. *Sol. Energy* 213, 118 (2021). https://doi.org/10.1016/j.solener.2020.11.041.
48. Y.Y. Luo, G.T. Duan, and G.H. Li, Resonant Raman scattering and surface phonon modes of hollow ZnS microspheres. *Appl. Phys. Lett.* (2007). https://doi.org/10.1063/12737398.
49. S. Sahoo and A.K. Arora, Laser-power-induced multiphonon resonant Raman scattering in laser-heated CdS nanocrystal. *J. Phys. Chem. B* 114(12), 4199 (2010). https://doi.org/10.1021/jp912103t.
50. Ö.B. Mergen and E. Arda, Electrical, optical and dielectric properties of polyvinylpyrrolidone/graphene nanoplatelet nanocomposites. *Opt. Mater.* 139, 113823 (2023). https://doi.org/10.1016/j.optmat.2023.113823.
51. S. Chander and M.S. Dhaka, Thermal evolution of physical properties of vacuum evaporated polycrystalline CdTe thin films for solar cells. *J. Mater. Sci.: Mater. Electr.* 27, 11961–11973 (2016). https://doi.org/10.1007/s10854-016-5343-2.
52. D.P. Sali and N.B. Chaure, Investigation of the effect of annealing conditions on electrodeposited CdTe thin films from non-aqueous bath. *Appl. Phys. A* 127, 1 (2021). https://doi.org/10.1007/s00339-020-04218-6.
53. E.M. Bacaksiz, B.M. Basol, M. Altunbaş, V. Novruzov, E.K. Yanmaz, and S. Nezir, Effects of substrate temperature and post-deposition anneal on properties of evaporated cadmium telluride films. *Thin Solid Films* 515(5), 3079 (2007). https://doi.org/10.1016/j.tsf.2006.08.026.
54. S. Chander and M.S. Dhaka, Impact of thermal annealing on physical properties of vacuum evaporated polycrystalline CdTe thin films for solar cell applications. *Physica E: Low Dimens. Syst. Nanostruct.* 80, 62 (2016). https://doi.org/10.1016/j.physe.2016.01.012.
55. A. Ukarande, S.M. Sonawane, S. Chaure, and N.B. Chaure, Wet-electrochemical growth of CdTe layers for photovoltaic applications. *J. Mater. Sci.: Mater. Electr.* 33(28), 22456–22468 (2022). https://doi.org/10.1007/s10854-022-09022-x.
56. L. Ma, Z. Wei, F. Zhang, and X. Wu, Synthesis and characterization of high-ordered CdTe nanorods. *Superlatt. Microstruct.* 88, 536 (2015). https://doi.org/10.1016/j.spmi.2015.10.014.
57. T.P. Rao, M.S. Kumar, and N.S. Hussain, Effects of thickness and atmospheric annealing on structural, electrical and optical properties of GZO thin films by spray pyrolysis. *J. Alloys Compd.* 541, 495 (2012). https://doi.org/10.1016/j.jallcom.2012.05.128.
58. C.L. Lin, F.H. Wang, H.S. Jhuang, and C.F. Yang, Effects of different annealing temperatures on the physical, optical, and electrical characteristics and chemical bonds of Ga and F co-doped ZnO films. *J. Mater. Res. and Technol.* 9(3), 6331 (2020). https://doi.org/10.1016/j.jmrt.2020.03.046.
59. E. Hasani and D. Raoufi, Comprehensive study of physical properties of cadmium telluride thin films: effect of post-deposition high annealing temperature. *Semicond. Sci. Technol.* 36(5), 055004 (2021). https://doi.org/10.1088/1361-6641/abe318.
60. S. Fiat and G. Çankaya, Evaluation of the hydrostatic pressure effect on Mn/p-Si Schottky barrier diode electrical parameters and interface states. *Mater. Sci. Semicond. Process.* 15(5), 461 (2012). https://doi.org/10.1016/j.mssp.2012.03.004.
61. H. Asıl Uğurlu, K. Çınar Demir, and C. Coşkun, The effect of thermal annealing on Ti/p-Si Schottky diodes. *J. Mater. Sci.: Mater. Electr.* 32(11), 15343 (2021). https://doi.org/10.1007/s10854-021-06084-1.
62. S. Paul, S. Sohal, C. Swartz, D.B. Li, S.S. Bista, C.R. Grice, Y. Yan, M. Holtz, and J.V. Li, Effects of post-deposition $CdCl_2$ annealing on electronic properties of CdTe solar cells. *Sol. Energy* 211, 938 (2020). https://doi.org/10.1016/j.solener.2020.10.015.
63. W. Mtangi, F.D. Auret, A. Chawanda, P.J. van Rensburg, S.M. Coelho, J.M. Nel, M. Diale, L. Van Schalkwyk, and C. Nyamhere, Thermal annealing behaviour of Pd Schottky contacts on melt-grown single crystal ZnO studied by IV and CV measurements. *Mater. Sci. Eng. B* 177(2), 180 (2012). https://doi.org/10.1016/j.mseb.2011.10.003.
64. A. Manna, S. Saha, and S.C. Saha, Fabrication and characterization of Al/n-CdSe schottky barrier under different annealing temperatures. *Chalcogenide Lett.* 14(7), 283 (2017).
65. A.A. Al-Ghamdi, M.S. Abd El-sadek, A.T. Nagat, and F. El-Tantawy, Synthesis, electrical properties and transport mechanisms of thermally vacuum evaporated CdTe nanocrystalline thin films. *Solid State Commun.* 152(17), 1644 (2012). https://doi.org/10.1016/j.ssc.2012.05.029.
66. I. Orak, K. Ejderha, E. Sönmez, M. Alanyalıoğlu, and A. Turut, The effect of annealing temperature on the electrical characterization of Co/n type GaP Schottky diode. *Mater. Res. Bull.* 61, 463 (2015). https://doi.org/10.1016/j.materresbull.2014.10.066.